Journal of
Marine Science and Engineering

MDPI

Article

Experimental and Numerical Investigation into the Effects of Air–Fluid Interaction on the Dynamic Responses of a Damaged Ship

Xinlong Zhang [1], Simone Mancini [2,3,*], Fei Liu [4] and Renqing Zhu [1]

[1] School of Naval Architecture and Ocean Engineering, Jiangsu University of Science and Technology, Zhenjiang 212000, China; just.zhangxinlong@just.edu.cn (X.Z.); zhurq@just.edu.cn (R.Z.)
[2] Department of Industrial Engineering, University of Naples "Federico II", Via Claudio 21, 80125 Naples, Italy
[3] Hydro & Aerodynamics Department, FORCE Technology, Hjortekærsvej 99, 2800 Kgs. Lyngby, Denmark
[4] Jiangsu Automation Research Institute, Lianyungang 222061, China; 18845098292@163.com
* Correspondence: simone.mancini@unina.it

Abstract: To accurately assess the dynamic stability of the damaged ship, this paper performs an experimental campaign and presents a feasible numerical method to analyze the effects of microscopic air–fluid interactions on the motion responses of the damaged ship. The numerical approach can be applied to solve the coupled hydrodynamic behavior between the flooding process and the motion responses of the damaged ship. The volume of fluid (VOF) method was applied to capture the interface of the free surface, while the dynamic fluid–body Interaction (DFBI) morphing technique was applied to deal with mesh adaption. In particular, the UDF (user-defined field) function was activated to realize the initial distribution of the free surface. Firstly, by comparing the experimental and numerical results, the reliability of visualizing the flooding process and dealing with the motion responses of the damaged ship was efficiently verified. The numerical flooding process was able to reproduce the hydrodynamic phenomenon well, including the flooding jet, interaction, and flow between adjacent compartments. The numerical roll motion curve of the damaged ship was consistent with that predicted in the model test, with an error in roll amplitude of no more than 4%. Secondly, based on the verified numerical method, it was seen from the results with different ventilation positions that not only the air compressibility due to varying levels of ventilation cannot be neglected in damage assessment, but also the position of the ventilation hole was crucial. This was because different positions will create different paths for the compressed air to overflow and affect air–fluid interactions. Thus, the flooding force and air-impacting force acting on the internal hull will be different. In conclusion, this paper introduces a new consideration in the damage assessment of ships.

Keywords: damaged ship; dynamic response; experimental verification; air–fluid interaction

check for updates

Citation: Zhang, X.; Mancini, S.; Liu, F.; Zhu, R. Experimental and Numerical Investigation into the Effects of Air–Fluid Interaction on the Dynamic Responses of a Damaged Ship. *J. Mar. Sci. Eng.* **2024**, *12*, 992. https://doi.org/10.3390/jmse12060992

Academic Editor: Md Jahir Rizvi

Received: 28 April 2024
Revised: 2 June 2024
Accepted: 10 June 2024
Published: 13 June 2024

Copyright: © 2024 by the authors. Licensee MDPI, Basel, Switzerland. This article is an open access article distributed under the terms and conditions of the Creative Commons Attribution (CC BY) license (https://creativecommons.org/licenses/by/4.0/).

1. Introduction

The significant hazards associated with ship collisions, grounding, and naval operations could pose a great threat to the safety of the hull itself and the personnel onboard. The dynamic flooding process and motion responses of a damaged ship are a multi-phenomenon engineering problem, which couples the shaking of the free surface in the damaged compartment with the mixing flow of the flooding water around the damaged opening. While the flooding water affects the motion of the damaged ship, the ship's motion will conversely affect the flooding process. Different from the quasi-static calculation of the damage stability, the transient flooding study in this paper not only focuses on the final flooded compartments and the final floating state of the damaged ship but also on the dynamic flooding process and motion variation of the damaged ship. The obtained flooding sequence and motion curve can provide valuable reference for rescue management and personnel evacuation. In order to accurately evaluate the dynamic performance of a

damaged ship in the transient flooding condition, various methods have been proposed in the past decades. These research methods can be roughly divided into three types: model testing, fast prediction based on potential flow theory, and numerical simulation methods based on computational fluid dynamics. Each method has its own advantages and disadvantages.

The model test is considered as the most direct and reliable research method, but it can be costly and time consuming. While the fast prediction method, based on the potential flow theory, is convenient, it is limited by multiple assumptions. It treats flooding water as a lumped mass, and it uses the hydrostatic model and quasi-static assumption to deal with the free surface. The free surface in the damaged compartment is usually assumed to be horizontal [1–3] and moves freely along a designated path [4,5] or according to the shallow water equations [6]. Furthermore, the fast prediction method is often used to calculate ship wave behavior using strip theory [1,2,6] or the panel method [3–5]. This method is generally accurate for low-frequency ship motion but may struggle with solving transient flooding or the violent shaking due to the nonlinear hydrodynamic characteristics. Therefore, computational fluid dynamic methods based on the finite volume method (FVM) and smoothed particles hydrodynamics (SPH) are widely applied. Numerical simulation methods have unique advantages in dealing with irregular geometric hulls, water viscosity, and air compressibility. Their good visualization capability can also assist in the dynamic analysis of damaged ships. Combining the research content in this paper, the following introduction reviews the model test and the numerical methods based on computational fluid dynamics.

1.1. Review of the Model Test Approach

The model test can not only provide reliable conclusions, but also the obtained experimental results can be used as a basis for the verifying the fast prediction method and the numerical simulation method. For the still water model test, Manderbacka et al. [7] conducted roll decay and transient flooding tests for a typical box barge, collecting experimental data such as the flooding height, initial metacentric height, and roll angle. Based on the quantitative analysis, the water ingress in the flooded compartment effectively dampens the roll motion of the damaged ship. Further analysis of the flooding process and motion responses reveals that the baffle obstructing the damaged compartment leads to asymmetric flooding, resulting in a significant roll angle for the damaged ship. Rodrigues et al. [8] measured the discharge coefficient of various opening geometries by conducting the progressive flooding test in still water. This would improve the accuracy of the damage assessment. Siddiqui et al. [9] also conducted a forced heave motion test on a hull model with a rectangular opening. The experimental results show the effects of tank shaking and resonance on the hydrodynamic characteristics of the damaged ship. It can be seen that the shallow water resonance phenomenon in the damaged compartment will create a large local load, and air compression has a significant influence on the entire flooding process.

In order to further study, the effects of air compression on the dynamic characteristics of a damaged ship, Ruponen et al. [10] conducted a full-scale test on a decommissioned ship. The results showed that compressed air in the flooding compartment delays the flooding process. Through a series of model tests with varying ventilation levels, it was found that the length of the ventilation duct, as well as possible bends and valves, were not adequately accounted for in IMO Resolution MSC.245 (83) [11], resulting in an oversimplification of the full ventilation ratio.

Considering the effects of wave loads on the motion responses of a damaged ship, Korkut et al. [12] tested the six degrees of freedom motion in a damaged ro-ro ship in head waves, beam waves, and quartering waves with different wave heights and frequencies. The results show that damage has an adverse effect on the motion responses of the ship model. However, this also depends on the wave direction and frequencies. Lee et al. [13] performed a test analysis on a damaged passenger ship. The test items included the roll decay of the ship in still water and the six degrees of freedom motion of the intact ship

in regular waves. The results can be used to analyze the effects of flooding water on rolling damping in the damaged ship. Furthermore, the data obtained can be used as a benchmarking reference for verifying the reliability of other numerical methods. Domeh et al. [14] previously studied the effects of compartment permeability and layout on the motion responses of the damaged ship. The test results indicate that, for a stationary damaged ship, compartment permeability has little effect on the pitch and heave motions of the ship, which is consistent with the conclusion from Santos et al. [15]. When a damaged ship sails with a forward speed, the compartment permeability has a greater influence on the pitch and heave motions of the ship than the internal layout of the damaged compartment. Based on Safe Return to Port regulations, Lim et al. [16] monitored the forward speed and motion responses of the damaged ship in different wave conditions in order to analyze its propulsion and maneuverability. The test results show that following waves will result in a higher speed for the damaged ship. Furthermore, the flooding water in the flooding compartment creates significant resistance for the ship, reducing its forward speed by 28% in head waves and 13% in following waves compared to an intact ship. Similarly, Bašić et al. [17] conducted a study on a damaged model with a bottom opening. The results show that the total resistance of the damaged ship increased by 27% compared to an intact ship, greatly impacting its propulsion efficiency when returning to port. Regarding to the influence of different damage locations, Acanfora et al. [18] investigated the roll motion of the damaged ship in still water and regular beam waves. The test results show that the roll behavior of the damaged ship is affected not only by the size of the damage opening but also by the location of the damage opening. Even if the final equilibrium of the damaged ship is consistent, the RAO (response amplitude operator) factor and roll decay characteristics would vary depending on the location of the damage opening.

Damage flooding in the compartments not only affects the motion response of the damaged ship but also impacts the load and bending moment on the hull. In their experiments, Lee et al. [19] measured the hydrodynamic load on a damaged ship in waves. The results demonstrate that compared to an intact ship, the damage opening changes the distribution of the hydrostatic bending moment and the wave bending moment. It can also be observed that although no structural damage occurs on the structure sections, the load acting on these structures is much larger than the designed load in the intact condition. Begovic et al. [20] analyzed the total load of the intact and damaged DTMB 5415 ship in regular waves at zero forward speed. This test was conducted based on previous model tests described in Begovic et al. [21]. The results show that when the wave frequency is close to the natural frequency of the ship, the vertical shear and bending moment of the ship are not influenced by the wave amplitude. Additionally, when the wave amplitude ranges from 0.8 to 1.5, the vertical shear force exhibits a noticeable second harmonic within a certain frequency range. Ćatipović et al. [22] carried out two sets of tests on a damaged hull. Firstly, they measured the rigid body motion of the intact and damaged ships in irregular waves with a small forward speed. The results showed that the damaged ship has greater heave motion, while the intact ship has greater pitch and roll motion. Secondly, they measured the motions and vertical wave moment of a segmented model in regular waves. By comparing the results of the intact and damaged ships, it can be seen that the vertical bending moment of the damaged ship will be greater than that of the intact ship. To analyze the effects of the load and bending moment increment on the damaged ship's structure, Jalonen et al. [23] conducted leakage and collapse tests on the ship's watertight structure to determine the pressure head of the non-watertight structure. From the test results, it can be concluded that the ultimate pressure head of the non-watertight structure on the ship is between 1.0 m and 3.5 m.

Generally, the model tests of the damaged ship in still water and waves have been extensively studied. The experimental methods and procedures described in the literature provided valuable references for the model tests in this paper. However, for the current model test, it would be worthwhile to further study the visualization analysis of the

flooding process. The dynamic flooding process would be helpful in assessing the flooding development and explaining the motion responses of a damaged ship.

1.2. Review of the Numerical Method

In recent years, with the development of high-performance computers, numerical simulations using the finite volume method and smooth particle method have greatly improved the study of hydrodynamics in damaged ships. They are capable of handling irregular hull geometry and taking into account the effects of nonlinear factors on calculation results. These nonlinear characteristics are primarily related to water viscosity, such as vortex generation, turbulent boundary layers, and viscous roll damping. Additionally, numerical simulations can also consider the impact of air compressibility on the flooding process and the motion responses of the damaged ship by defining air as an ideal gas.

In their numerical simulation of still water, Begovic et al. [24] employed STAR-CCM+ to simulate the roll decay of both intact and damaged ships utilizing two symmetric flooding compartments. The overset mesh technique was used for mesh adaption, while time, grid, and turbulence sensitivity analysis provided valuable references for similar damage simulations. Through comparison with experimental results, the reliability of the numerical simulation method was successfully validated.

Zhang et al. [25] also utilized the overset mesh technique to analyze the effects of different damage locations in the same compartment on the flooding process and motion responses of a damaged ship. The simulation results reveal that the heave and pitch motion of a damaged ship would not be impacted by the damage opening. However, for the roll motion of a damaged ship, the impact caused by the flooding from the bottom opening is greater, and the roll amplitude in the same roll period is larger. This can provide a new reference for the traditional calculation of damage stability, specifically the effects of damage information on the assessment of damage stability should be dynamically considered. Based on URANS solver and the volume of fluid (VOF) method, Zhang et al. [26] studied the effects of symmetric and asymmetric flooding on the dynamic stability of a damaged ship. From the visualization of the flooding process, it can be observed that the obstruction of the longitudinal bulkhead will cause the flooding water to only accumulate on the damaged side. In this scenario, the damaged ship will incline towards the damaged side, resulting in a large roll angle and threatening the safety of the ship. However, for symmetric flooding, the ingress of water flowing into the intact compartment can help the damaged ship maintain a good floating state. This allows the damaged ship to safely return to port as long as it does not sink due to excessive flooding water.

Taking into account air compressibility in the flooding compartment, Gao et al. [27] studied the effects of compression characteristics on the flooding process and motion responses of a damaged ship using ANSYS Fluent 12.0. The dynamic mesh technique was used to account for the motions of a damaged ship. The simulation results showed that as the difficulty of escaping compressed air increases, the flooding velocity at the damage opening will decrease. In the closed scenario, the air cushion formed by the compressed air will prevent the flooding water from flowing into the damaged compartment. This further explains the importance of maintaining compartment air tightness to slow down the flooding velocity and reduce the final amount of flooding, especially when predicting excessive flooding and the potential for the ship to sink.

To study the dynamic characteristics of a damaged ship in waves, Sadat-Hosseini et al. [28] used a URANS solver to simulate the motion responses of a damaged ship in regular beam waves with different wavelengths. The simulation results showed that except for the parametric roll condition that displayed large harmonic responses for the intact ship, the second-order responses were small for both the damaged and intact ship. Haro et al. [29] utilized the CFD Ship-Iowa software V4.5 and SUGGAR++ to simulate the motion responses of a damaged ship in head waves and following waves. When compared with experimental results, the numerical prediction of pitch and heave motion showed good accuracy. However, the numerical results overestimated the roll motion at the natural

frequency and forward speeds in head waves. Ming et al. [30] used the smoothed particle method to study the hydrodynamic behavior of a damaged compartment in beam waves. The simulation results demonstrated that compared to the flooding process in still water, the wave excitation intensified the flooding sloshing. When the beam waves were directed towards the damaged side of the ship, the wave force caused the damage opening to move away from the free surface. As a result, the flooding speed at the damage opening decreased and could even lead to flooding stagnation. Conversely, when the beam waves were directed towards the intact side of the ship, the wave force caused the damage opening to be submerged deeper. This increased the hydrostatic pressure at the damage opening, leading to a higher flooding speed. Gao et al. [31], using the RANS solver and VOF method, analyzed the effects of compartment layout and wave height on the flooding process and motion responses of a damaged ship, explaining the capsizing principle of a damaged ship in waves. Additionally, due to the importance and necessity of researching damaged ships in ice floes, Zhang et al. [32] combined computational fluid dynamics and the discrete element method to investigate the impact of ice floes and their sizes on the flooding process and motion responses of a damaged ship. The research method will serve as a valuable reference for further studies on the safety of polar damage ships.

Although simulations based on the CFD method require significant computation effort, they provide great convenience in studying complex hydrodynamic problems of damaged ships. In particular, visualizing the flooding process is irreplaceable in other research methods. This allows for clear observation of the progression of flooding and accurate prediction of the time that each compartment will flood. Additionally, the visualized flooding process can serve as a basis for explaining the motion responses of a damaged ship. The related flooding information is also valuable for making damage rescue management decisions.

1.3. Main Contents of This Study

This paper focuses on the transient flooding of a damaged ship, introducing numerical methods in detail. In order to validate the reliability of the proposed numerical modelling method, an innovative experimental campaign was carried out to perform the verification analysis. The main content of this paper is as follows: Section 2 introduces the numerical method and presents the key UDF simulation settings, while Section 3 introduces the experimental campaign, including the test scenario and the test model. Section 4 performs the verification analysis on different flooding forms, including symmetric and asymmetric flooding. Based on the verified numerical method, Section 5 investigates the effects of air–fluid interaction on dynamic responses of a damaged ship. Finally, conclusions and further work are enclosed in Section 6. Overall, the content of this paper can provide valuable engineering reference for the numerical method and experimental investigation of a damaged ship.

2. Introduction of the Numerical Method

In the authors' previous publications on the transient flooding of a damaged ship, some basic numerical theory was elaborated upon in detail, including the governing equations of fluid flow, the ship motion, and the VOF method. In this case, this section focuses on some key numerical settings, specifically the introduction of the user-defined function (UDF) approach to realize the initial water–air distribution in the irregular compartment. Implementation is an important prerequisite for performing the flooding study using the CFD software STAR-CCM+ 18.04. Additionally, this section introduces the applied motion specification, aimed at better dealing with the mesh adaptation of the free surface.

2.1. User Define Function

In the numerical simulation of an intact ship, the simulation operation can be performed by using a closed shell or entity to define the hull. However, for the simulation of damage flooding in this paper, the flooding compartments need to be divided by plates of varying thicknesses. A Boolean operation will connect the potential flooding compart-

ments with the external simulation domain and fill them with flooding water in the initial condition, but transient flooding will not be realized. In this case, it is necessary to conduct development of the simulation program through a user define function, making the potential flooding compartments be filled with air at the initial stage. This section presents the expression form of the user define function for damaged compartments with regular and irregular geometric shapes. It is worth noting that this approach is applicable to a single simulation domain; multiple simulation domains would require additional settings.

2.1.1. Regular Compartment Geometry

Figure 1 presents three flooding scenarios with different damage locations. It can be observed that regardless of whether the damage opening is above, at, or below the free surface, the damaged compartment is flooded in the initial condition, thus preventing the realization of transient flooding simulation.

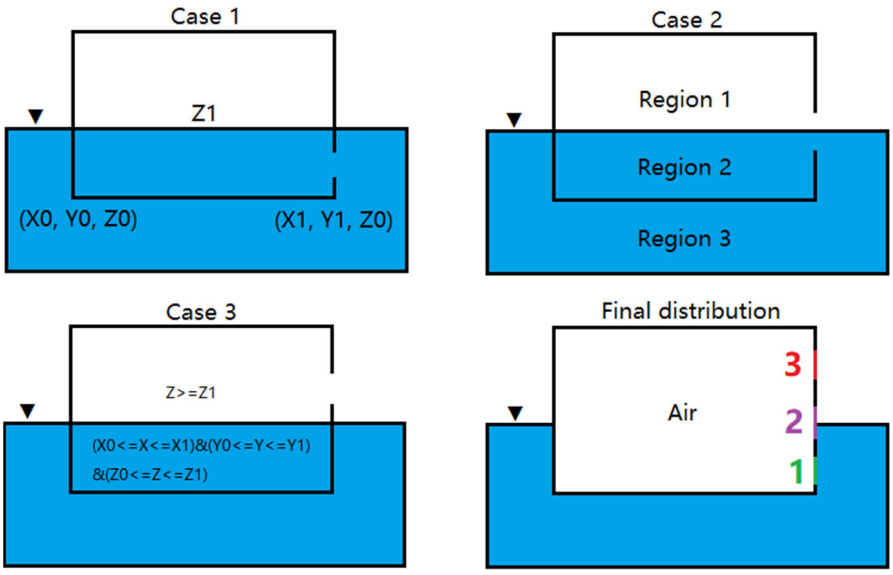

Figure 1. Schematic diagram of the free surface in the flooding compartment (Zhang et al. [33]).

For the rectangular compartment geometry depicted in Figure 1, the entire domain can be divided into three regions by the free surface and bulkheads of the damaged compartment. Region 1, located above the free surface, is filled with air in the initial condition. Region 2, situated below the free surface and outside the damaged compartment, is initially filled with water. The remaining space, Region 3, below the free surface and in the damaged compartment, should be filled with air instead of water in the initial condition. To address this limitation, a UDF is necessary.

The basic concept is to use the four angular coordinates of Region 2 to form six faces. The space created by these six faces should be the same as Region 2. In the initial condition, the phase condition at Region 2 is set to be air. This allows for the final distribution scenario as shown in Figure 1. Regardless of the relative position between the damage opening and the free surface, the damaged compartment will always be filled with air. As a result, at the start the simulation, the dynamic water ingress will continuously flood the damaged compartment, causing the damaged ship to move due to the flooding force.

The specific definition of the field function is provided in Equation (1). It is worth noting that in the process of the field function, reference to the self-developed language of STAR-CCM+ is mandatory. As shown in Equation (1), $$Position[0] represents the x-direction, $$Position[1] represents the y-direction, and $$Position[2] represents the z-direction. The value of 0 indicates that the volume fraction of water in the defined region is 0, which represents the air phase. ${VolumeFractionHeavyFluidWave0} is utilized to define the volume integral of water. Notably, the function introduced in Equation (1) is exclusively applicable to the rectangular compartment geometry. Other regular or complex

geometry shapes require a specified definition, which also explains the necessity of the following Section 2.1.2.

$$(\$\$Position[2] \geq Z1)||(X0 \leq \$\$Position[0] \leq X1)\&\&Y0 \leq Positon[1] \leq Y1\&\&Z0 \leq \$\$Position[2] \leq Z1?0 : \${VolumeFractionHeavyFluidWave0}\} \quad (1)$$

2.1.2. Irregular Compartment Geometry

Section 2.1.1 provides UDF definition format for the regular compartment geometry. However, when dealing with damaged compartments featuring complex curvature, the linear definition of the compartment's geometry shape becomes impractical. In such cases, a more efficient method is needed to define the space inside the damaged compartment. During the numerical operation, grids in the flooding compartments can be picked up by a cell set function. The general operation is shown in Figure 2. First, a small expansion cell is established in the damaged compartment. Then, through repeated operations of growth and contraction, the expanding cell would fill with the flooding compartment. The generated cell set would be named according to the procedure order. It is worth noting that UDFs need to be defined according to the cell set number's name. Equation (2) shows a general form of a UDF only involving one "CellSetVar". The definition of UDFs needs to strictly follow the internal language format of STAR-CCM+ software 18.04. Otherwise, the simulation program will not be able to recognize the defined UDF.

$$\${CellSetVar_1}?0 : \${VolumeFractionHeavyFluidWave0}\} \quad (2)$$

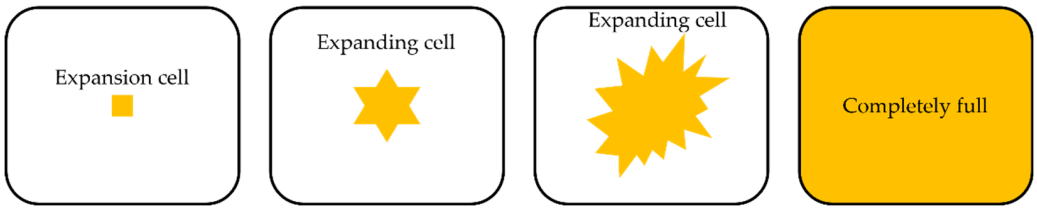

Figure 2. Generation process of the cell set.

2.2. Motion Specification of the Damaged Ship

This paper aims to confirm the reliability of the numerical modeling method in addressing the nonlinear coupling of flooded scenarios and damaged ships from two perspectives: the dynamic flooding process and the motion responses of the damaged ship. Section 2.1 discusses the limitations of simulating transient flooding scenarios. The purpose of this section is to introduce how the simulation handles the mesh adaptation of the free surface and the movements of the damaged ship.

In numerical simulations, two approaches can be used to handle the movement of the damaged ship: DFBI rotation and translation, and DFBI morphing. While these approaches are both suitable for adjusting the mesh, they differ in their solutions. As shown in Figure 3, a mesh refinement block is placed around the free surface to ensure simulation accuracy. In the simulation with DFBI rotation and translation (Figure 3a), the refined background region moves with the damaged ship while the free surface remains still. This guarantees accuracy for small inclination angles but may lead to numerical errors and instability when the damaged ship inclines at a large angle.

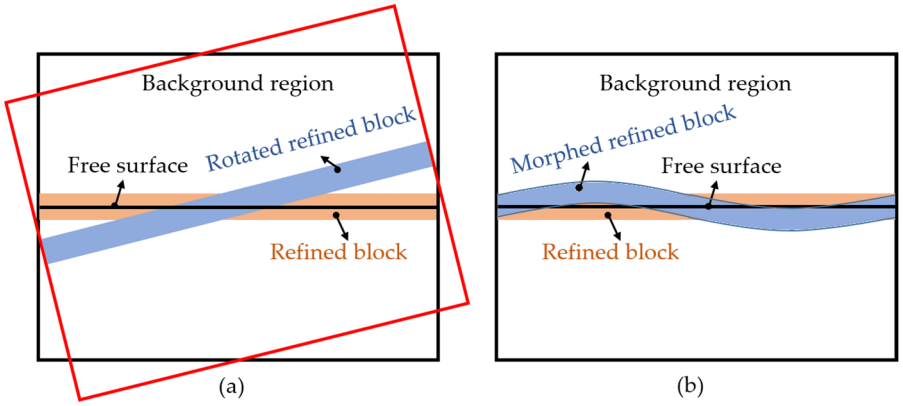

Figure 3. Motion specification: (**a**) DFBI rotation and translation; (**b**) DFBI morphing.

In contrast, for the simulation with DFBI morphing shown in Figure 3b, the discretized background region is always stationary, but the mesh within the domain morphs with the motions of the damaged ship, including the mesh in the refined block around the free surface. As long as the damaged ship does not experience excessive inclination motion, the free surface will mostly remain within the refined block. Compared to the simulation with DFBI rotation and translation, although the simulation with DFBI morphing requires more computational effort, it offers greater stability and more accurate numerical results. Considering these factors, the simulations in this study employ the DFBI morphing technique.

2.3. Simulation Domain and Mesh Generation

As depicted in Figure 4, the damaged ship is placed in the virtual simulation domain segmented by the free surface. To prevent any transient heave motion of the damaged ship, the draft of the damaged ship should be set accurately according to the actual weight. In the numerical simulation, the draft can be determined by the pre-simulation, which only releases the freedom in the Z direction. Subsequently, based on the obtained results, the actual draft can be calculated. In this paper, the weight of the test model was 126.84 kg, and the corresponding draft was 0.20971 m. Practical Guidelines for Ship CFD Applications [34], Mancini et al. [35], and Handschel et al. [36] provide insights into domain sizes relative to the ship length, as labeled in Figure 4.

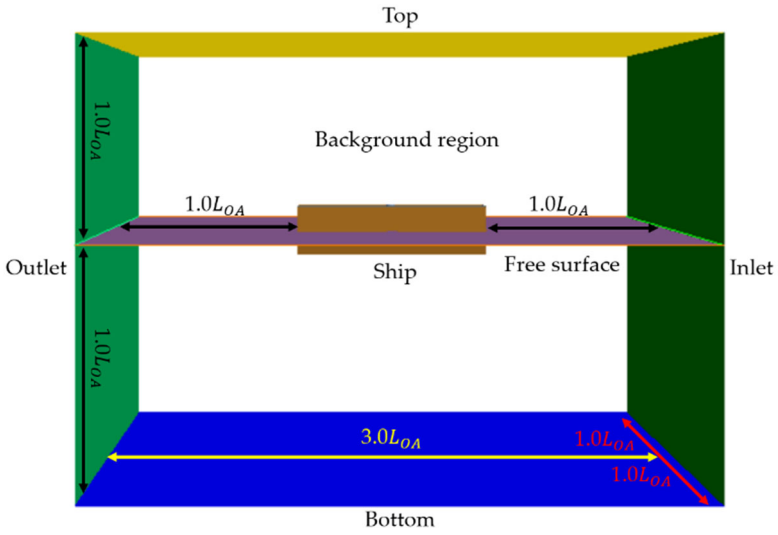

Figure 4. Domain sizes and boundary conditions.

Since the simulation of damage flooding in still water will not produce a severe wall reflection phenomenon, this paper adopted a smaller domain size. This approach guarantees simulation accuracy and reduces computational effort. Moreover, to define

the interaction between the fluid flow and the boundary, the inlet, outlet, top, and bottom boundaries of the domain in Figure 4 were set as velocity inlets. The hidden side boundaries were designated as pressure outlets.

Different from the mesh generation in the simulation of the intact ship, simulating the damaged ship requires further consideration of the internal geometry of the flooding compartments. The entire mesh generation process can be divided into three steps: mesh wrapping, surface remeshing, and volume mesh generation. Among these steps, the execution of the latter must build upon a solid foundation established by the former. Otherwise, mesh quality cannot be ensured.

Firstly, by ensuring that there are no overlapping surfaces on the ship surface, the wrapper function can repair small discontinuities on the surface and only carries out wrapping operations on potential flooding zones. This explains why the simulation results in this paper only display the flooding compartments, greatly reducing mesh complexity due to the geometric details of the non-flooding zones.

Then, based on the hull geometry generated by the mesh wrapper, an accurate remeshed surface is a prerequisite for generating good volume mesh. During the remeshing process, areas with significant curvature require additional refinement blocks. As shown in Figure 5, the circular ventilation hole on the main deck retains its original geometry. Additionally, circular openings in internal compartments also requires a refinement block. Generally, the most important principle in remeshing operations is to adjust the remeshed size according to a scale of $\sqrt{2}$ until the remesh shape of the local part is the same as the original geometry.

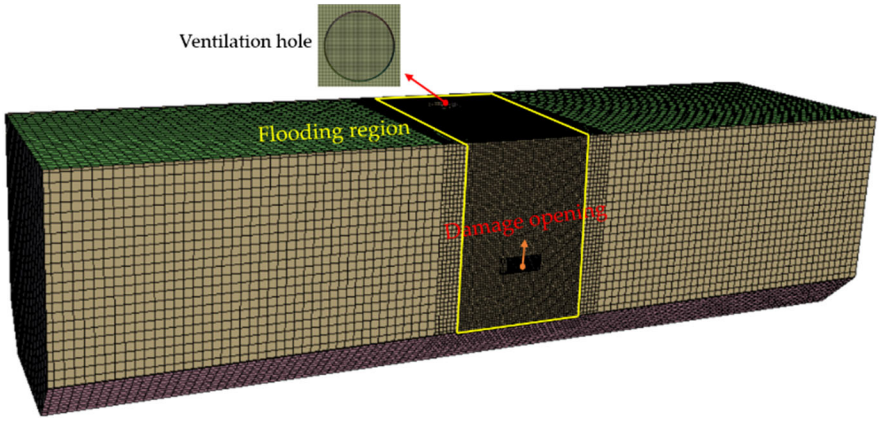

Figure 5. Mesh details of the hull surface and flooding region.

Finally, based on the hull geometry generated by the remeshing process, as shown in Figure 6, hexahedral meshes were used to spatially discretize the computation domain. It was observed that the mesh near the damaged ship was refined, while a relatively coarse mesh was applied in the region farther from the damaged ship. Moreover, to ensure simulation accuracy, certain regions need to be refined independently, including the free surface region and the mesh transition region around the hull. The refinement block around the free surface must ensure that as the damaged ship moves under the flooding forces, the free surface remains within the original refinement block. Its thickness requires a pre-simulation. The purpose of setting a mesh transition region around the hull is to prevent the grid from self-intersecting or causing a large residual value due to significant mesh size changes. Additionally, as shown in Figure 6, in order to capture the hydrodynamic details caused by the solid–liquid interactions, the volume mesh in the flooding compartments also requires refinement. Table 1 presents detailed mesh sizes.

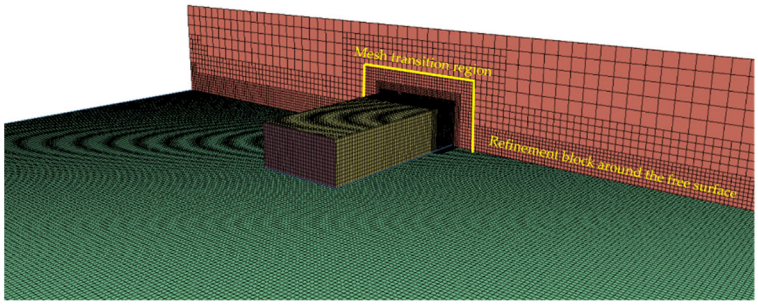

Figure 6. Mesh details of the domain.

Table 1. Mesh sizes of the hull surface and the local region.

Parts	Wrapper Size (m)	Remesher Size (m)	Trimmer Size (m)
Hull surface	0.010	0.010	None
Ventilation hole	0.010	0.005	
Damage opening	0.010	0.010	
Internal opening	0.010	0.005	
Flooding region	None	None	0.005
Transition region			0.010
Free surface region			0.025

2.4. Physical Models and Solver Setup

This section introduces the physical models adopted in the simulations to define the solution approach of the governing equations in the domain. Considering stability and accurate prediction, the realizable k-ε two-layer turbulence model was applied to solve the Reynolds stress problem. This model offers a good compromise between robustness, computational cost, and accuracy. The free surface was modeled using the two-phase VOF approach with a high-resolution interface capturing (HRIC) scheme based on the Compressive Interface Capturing Scheme for Arbitrary Meshes (CICSAM) introduced by Ubbink [37] and developed by Muzaferija and Peric [38]. The HRIC scheme is currently the most successful advection scheme and is extensively used in many CFD codes, as reported in Wackers et al. [39]. The standard configuration of the HRIC scheme depends on the local Courant–Friedrichs–Lewy number (CFL) on the air–water interface. During the simulation process, to eliminate the effects of the reflecting waves on the numerical results, the wave damping model needs to be set at the boundary. As shown in Figure 4, except for the top and bottom boundaries, the inlet, outlet, and side boundaries were specified with the damping zone. For flooding simulation in still water, a damping zone equivalent to 0.5 of the ship length is considered sufficient.

Additionally, an implicit solver has been used to find the field of all hydrodynamic unknown quantities, in conjunction with an iterative solver to solve each time step. Based on the time-step sensitivity analysis, the simulation in this paper applied a time step of 0.002 s with 10 inner iteration steps. Meanwhile, the software utilized a Semi Implicit Method for Pressure Linked Equations (SIMPLE) to conjugate pressure and velocity field, as well as an Algebraic Multi-Grid (AMG) solver to accelerate the convergence of the solution. A segregated flow solver approach was employed for all simulations.

3. Introduction of the Experimental Campaign

3.1. Test Scenario

Considering the requirements of the flooding tests on the experimental basin, including the experimental equipment and test functions, Figure 7 illustrates the test scenario. The entire test preparation primarily involved the constructing of the experimental basin,

manufacturing of the test model, adjusting of the hosting equipment, and installing of the motion sensor and cameras. The objective of the experimental design was to carry out a flooding test of the damaged ship in still water with only one operator. Meanwhile, the motion responses and flooding process of the damaged ship can be recorded and saved by the experimental equipment.

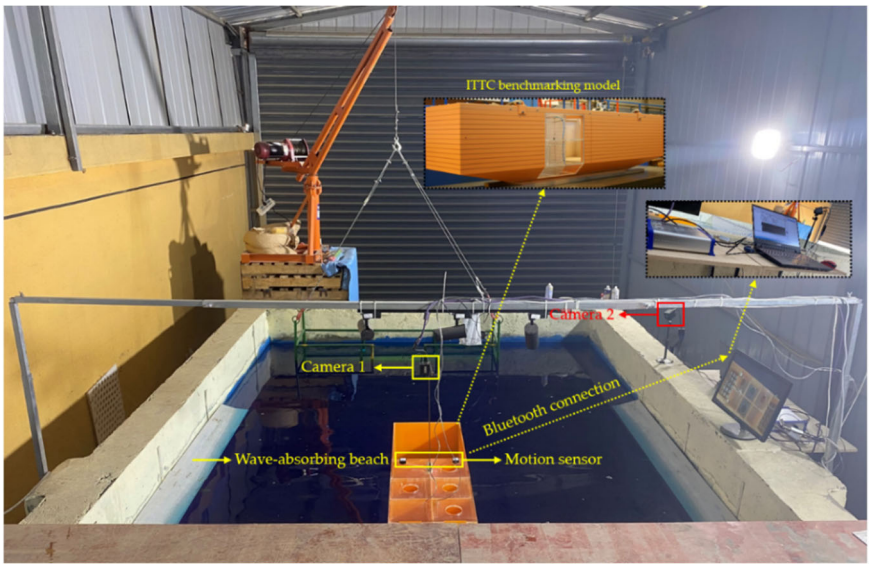

Figure 7. Schematic diagram of the test scenario.

3.1.1. Experimental Basin

The model tests were conducted in a custom-built basin with internal dimensions of 6 m × 3 m × 1.5 m, and a wall thickness of 25 cm. The side walls of the basin were reinforced with concrete and steel bars to prevent insufficient strength due to excessive water pressure. As shown in Figure 7, a platform spanned both sides of the basin wall, providing convenience for various operations such as scenario layout, positioning of the ship model, equipment power supply, and the transient release of the damage opening. Additionally, wave-absorbing barriers were installed along both longitudinal sides of the basin wall. These barriers were made of plastic plates with 5 mm apertures and were installed at an inclined angle. The principle of wave absorption operated in two main ways: firstly, the inclined barriers converted wave kinetic energy into gravitational potential energy, and secondly, the narrow space formed between the inclined beaches and the free surface inhibited the wave reflection. Overall, the installation of wave-absorbing barriers helped accelerate the stability of flow fluctuation caused by model lifting in and out.

3.1.2. Experimental Equipment

According to the requirements of numerical verification, the function design of the experimental equipment needs to be able to dynamically capture the flooding process and record the motion responses of the damaged ship. As shown in Figure 7, two identical motion sensors were symmetrically installed on the main deck of the damaged ship and connected to the specified instrument via Bluetooth®. One sensor was connected to a mobile device, and the data displayed on it can be used to determine whether the fluid flow and the ship meet the test conditions of still water. Only when the inclination angle of the damaged ship stops changing will the flow field reach a state of still water. The other sensor was connected to a computer where the motion data of the damaged ship can be saved in real time.

Furthermore, two cameras were separately installed on the damaged hull and the side wall of the basin. Camera 1 fixed on the main deck can capture the hydrodynamic behaviors in the flooding compartments. The dynamic flooding process can be used to validate the reliability of the VOF method in capturing the free surface. Camera 2 fixed on the side

wall of the basin can capture the inclination process of the damaged ship in the geodetic coordinate. The recorded video can be used to analyze the final floating condition of the damaged ship. The relevant results will be presented in the extended study in Section 5.

3.1.3. Operation Procedure

As mentioned in Section 3.1, the innovation of the tested model in this paper is that the entire test can be performed with only one operator. In this case, the procedure for model testing needs to be specially designed and planned in detail. Figure 8 presents the main procedure for the model test. During the preparation stage, the test model and the external flow field need must meet the requirements. First of all, in order to achieve the transient flooding, the damaged opening needs to be sealed first. Then, with the assistance of the lifting equipment, the test model will be lifted in the basin and located in the middle of the basin. After turning on the motion sensors and powering camera 1, the flow field must become stable enough to reach the condition of still water. The consistency of the external flow field is important to ensure the rationality of the numerical reliability analysis.

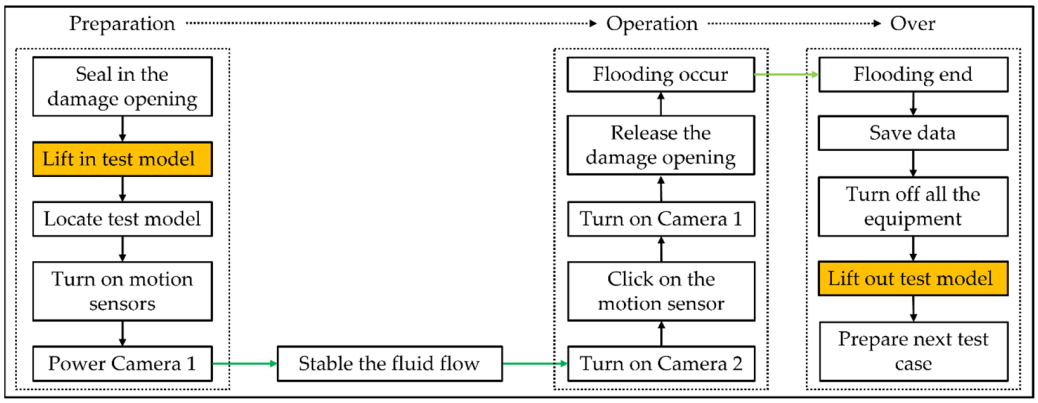

Figure 8. Main procedure of the model test.

During the operation stage, the operator needs to turn on the recording function of the experimental equipment in sequence. As shown in Figure 8, the direction of the arrows represents the operating sequence for turning on the experimental equipment. When all the equipment is ready, the damaged opening will be released, signaling the start of the flooding test. Gradually, water will enter the potential compartments until the flooding is over. Additionally, due to the repeatability of multiple tests in this paper, the damaged ship will be lifted out of the basin for the next case.

3.2. Test Model

As seen in Figure 7, the test model was scaled and modified from the ITTC benchmarking model. The modified model takes on the shape of a box body, which will facilitate the determination of the physical properties of the test model in Section 3.2.2. Additionally, the regular geometric shape is easy to model the test ship in 3D CAD design software (Solidworks 2019), which is valuable for other researchers to validate through the test data obtained in this paper. This section introduces considerations for the compartment division, ventilation design, and the calculation approach of physical properties.

3.2.1. Compartment Division and Ventilation Design

Combining Figures 7 and 9, it can be seen that the tested model is composed of three regions: the counterweight regions (before and after the model) and the flooding region.

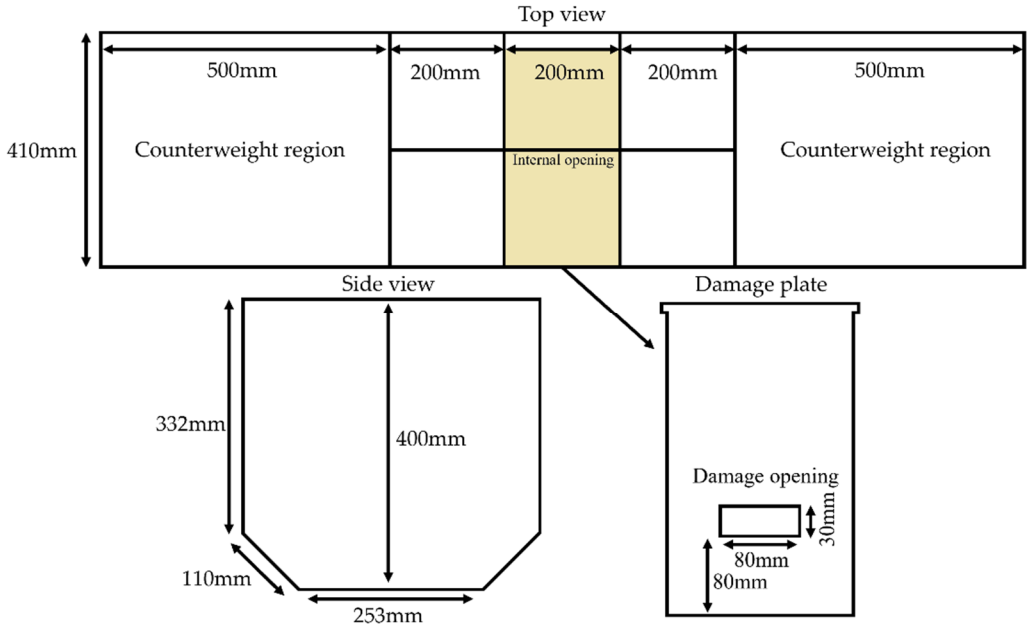

Figure 9. Schematic diagram of the compartment division.

This flooding region is divided into six compartments, while the tests only allow for up to two potential compartments to be flooded. Figure 10 presents all the flooding cases discussed in this paper, including asymmetric flooding in a single damaged compartment and symmetric flooding in two adjacent compartments. To verify the reliability of the numerical method proposed in this paper, Cases 1 and 3 (100% ventilation) were experimentally tested in Section 4 for validation analysis. Considering that different positions of the ventilation hole may result in different outflow paths of compressed air, and assuming that the size and position of the damage opening remain unchanged, Case 2 (with the ventilation hole on the damaged side) and Case 3 (with the ventilation hole on the intact side) were applied in Section 5 to numerically investigate the effects of air–fluid interaction on the motion responses of the damaged ship.

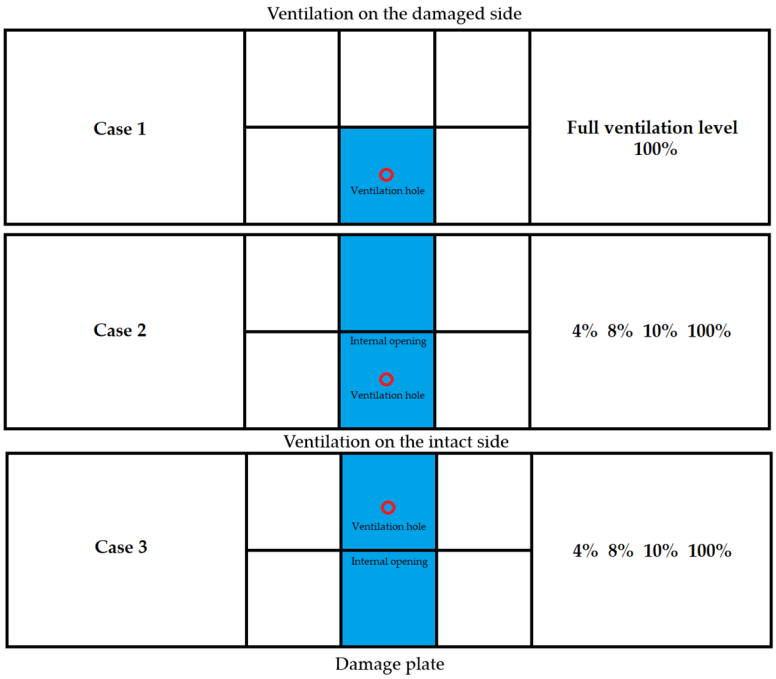

Figure 10. Schematic diagram of the ventilation design.

According to the ventilation assumption in IMO, Resolution MSC.362 (92) (2013) [11], a tank is considered fully vented if the total area of the air pipes is at least 10% of the area of the crossing-flooding device. Thus, a ventilation ratio of 10% is used as a reference in ventilation design. For the flooding region, the damaged opening acts as the crossing-flooding device and the ventilation hole acts as the air pipe. Based on the size of the damaged opening (80 mm × 30 mm, as shown in Figure 8), four ventilation levels are defined on the ship model deck (4%, 8%, 10%, and 100%). This leads to corresponding ventilation hole diameters of 11.1 mm, 15.6 mm, 17.5 mm, and 55 mm, respectively. Finally, in this paper, to completely eliminate the effects of compressed air on the dynamic performance of the damaged ship, the circular ventilation hole diameter in the full ventilation scenario was set to 80 mm.

3.2.2. Physical Properties

In order to ensure comparability between numerical and test results, the simulation program requires an accurate hull geometry, as well as the actual physical properties of the test model, including weight, draft, center of gravity, and moment of inertia. While the weight and draft can be determined by weighing and pre-simulation, the center of gravity and moment of inertia require a more complex process. As shown in Figure 11, the center of gravity was calculated by using an inclination experiment, and the specified theory can be found in the report by Ruponen [40], which outlines the solution for the initial metacentric height and the use of linear regression with experimental data. Additionally, the moment of inertia can be measured using 3D CAD design software (Solidworks 2019). It should be noted that too much homogenization can lead to errors, so this approach is only applicable for test models with mostly homogeneous parts. For the test model used in this paper, the main errors are from motion sensors and the camera. However, their small ratio to the total weight of the ship model allows for an acceptable level of measurement accuracy.

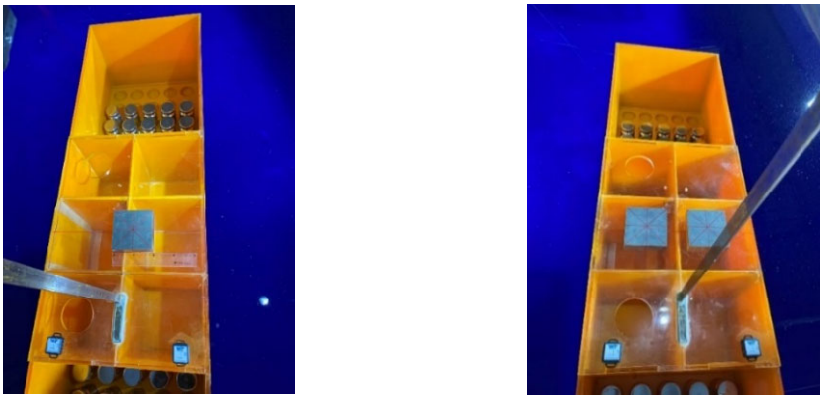

Figure 11. Test scenario of the inclination experiment.

Table 2 displays the physical properties obtained for the ship model. Furthermore, the final draft of the ship model was 0.329 m, with the additional ballast provided by the counterweights.

Table 2. Physical properties of the ship model.

Parameter	Weight (kg)	Vertical Height of Gravity of Center (m)	L_{xx} [kg/m^2]	L_{yy} [kg/m^2]	L_{zz} [kg/m^2]
Value	126.840	0.157	3.054	28.473	29.085

4. Numerical Reliability Analysis

Considering the challenge of numerical modelling methods in dealing with the motion responses of damaged ships with different forms of flooding, this paper performed reliability analysis on symmetric and asymmetric flooding. The aim was to analyze the

accuracy of the numerical method in solving small inclination and large inclination motions. Additionally, to verify the effectiveness of the mesh configuration in the simulation, this section also conducted the mesh sensitivity analysis in the symmetric flooding scenario, including the coarse mesh case (cells number: 707,419), the medium mesh case (cells number: 1,180,853), and the fine mesh case (cells number: 2,346,058). Considering the delaying effect of compressed air on the flooding process, the flooding region of the damaged ship in the test scenario was provided with good ventilation.

As introduced in Section 2.2, the reliability of the numerical modelling method was verified from two aspects. On one hand, by comparing the hydrodynamic phenomena captured in the test and numerical simulation, the reliability of the VOF method in visualizing the flooding process can be verified. The main flooding behaviors include the flooding jet, interaction, and flow between adjacent compartments. On the other hand, by comparing the roll motion curves of the damaged ship in the test and numerical simulation, the reliability of the DFBI morphing technique in dealing with the motion response of the damaged ship can be verified. Although the damaged ship without any constraint can freely move in six degrees of freedom, it can be seen that most damaged ships capsize due to excessive roll angle. Taking this into account, this section only performed reliability analysis for the roll motion.

4.1. Symmetric Flooding in Two Adjacent Compartments

In Figure 12, the hydrodynamic phenomena captured in the model test and numerical simulation are compared. As the symmetric flooding scenario involves the mixed flow of water in multiple compartments, the flow process of the flooding water through the internal opening is also compared in Figure 12. This comparison aids in analyzing when the maximum amplitude value of the roll motion occurs. From Figure 12, it can be seen that the visualization simulation method effectively captured the jet behavior during the transient flooding stage, solid–fluid interaction behavior, and the mixed flow in the flooding compartments.

The numerical simulation accurately reproduced the macroscopic flooding process observed in the model test. It is worth noting that the video recording equipment used in the model tests was rigidly fixed on the ship's deck, resulting in static images. On the other hand, the free surface in the numerical simulation did not change with the movement of the ship's yaw motion, which explains the difference in images between the experimental and numerical results. The reliability of the numerical modelling method in visualizing the flooding process was verified through the macroscopic hydrodynamic behavior. However, due to limitations in test conditions and equipment configuration, it was unable to capture the microscopic details for comparison.

To ensure the reliability of the numerical modelling method in dealing with the motion responses of the damaged ship, Figure 13 compares the roll motion curves of the damaged ship in the model test and the numerical simulations with different mesh accuracies. Based on the overall variation trend and roll amplitude, the roll motion curves obtained in the numerical simulations were in good agreement with those obtained in the model test. Although the roll amplitude of the damaged ship was closer to the test value with the improvement of the mesh accuracy, the results shown in Figure 13 are sufficient to prove the mesh dependency on the numerical results in this paper.

When examining the overall trend, it is important to note that since adjacent compartments are connected by internal openings, there will be a sequential flooding in the affected region. The initial flooding stage results in water accumulating in the damaged compartment, causing the damaged ship to roll towards the affected side. Once the flooding water reaches the lower edge of the internal opening, it then enters the adjacent compartment, causing the damaged ship to roll towards the undamaged side. This explains why the curved motion of the damaged ship appears in a V-shape. Moreover, taking the fine mesh case as an example, the maximum roll amplitude of the damaged ship was 5.5 degrees. Comparing this with the 5.7 degrees obtained in the model test, the difference of only

0.2 degrees resulted in an error of 3.6%. This small difference highlights the reliability of the numerical method in dealing with the motion response of the damaged ship.

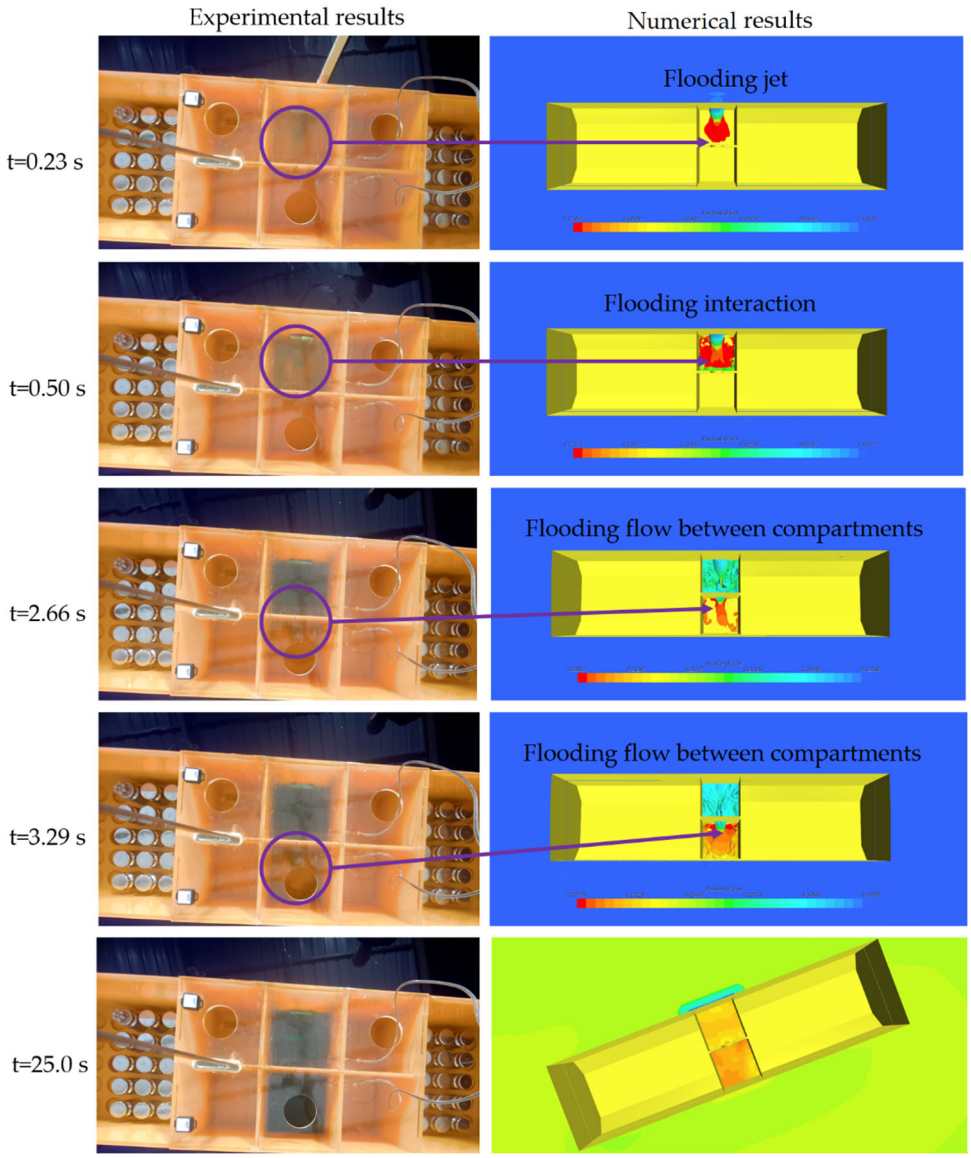

Figure 12. Comparison of the symmetric flooding process between the test and numerical results.

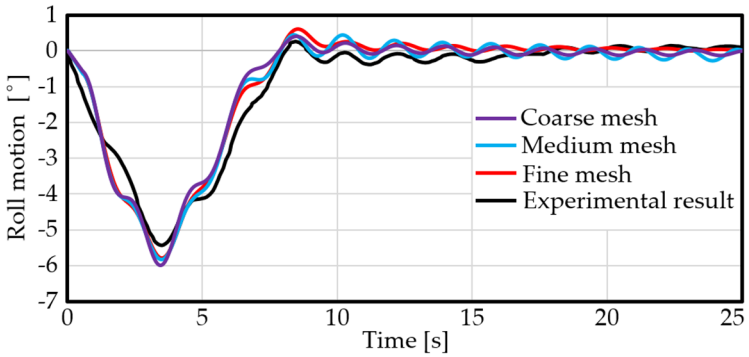

Figure 13. Comparison of roll motions between the simulation and test results for symmetric flooding.

By combining the flooding process shown in Figure 12 with the roll motion of the damaged ship shown in Figure 13, it can be seen that the maximum roll angle of the

damaged ship did not occur at the moment when the water ingress first flooded the adjacent intact compartment. Instead, it occurred after flooding had taken place in the adjacent intact compartment. In other words, the inclination moment generated by the accumulated flooding in the damaged compartment cannot cause the damaged ship to roll to its maximum angle.

As shown in Figure 13, the time at which the water ingress just flooded the intact compartment was around 2.66 s, but the time at which the maximum roll angle occurred was around 3.60 s. In order to clearly show the flooding distribution in these two moments, Figure 14 dynamically displays the flooding process. Compared with the asymmetric flooding in the damaged compartment at 2.66 s, although some water ingress flooded the adjacent compartment at 3.60 s, the restoring moment generated by the flooding water in the intact compartment was not sufficient to offset the inclination moment generated by the subsequent flooding in the damaged compartment. This explains why the maximum roll angle of the damaged ship occurred after the water ingress flooded the adjacent intact compartment. Moreover, it highlights the convenience of numerically visualizing the flooding process to explain the motion responses of the damaged ship.

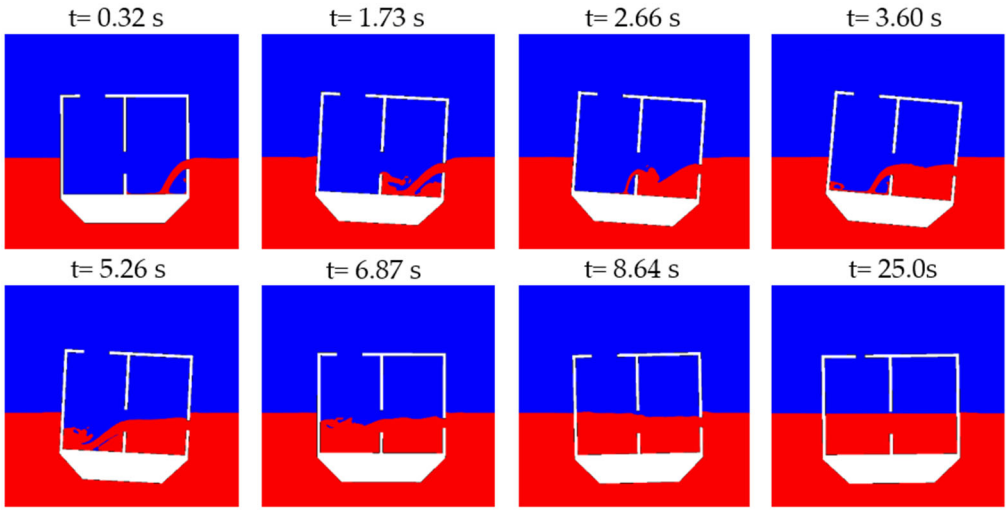

Figure 14. Flooding distribution at the typical flooding moments.

4.2. Asymmetric Flooding in One Compartment

As mentioned earlier, this paper performed reliability analysis on symmetric and asymmetric flooding. This section further validates the accuracy of the numerical method in dealing with large inclination motion of damaged ships. To capture the hydrodynamic behavior in the flooding compartment in detail, the fine mesh configuration validated in Section 4.1 was used. The cell number was 2,056,500. Figure 15 compares the asymmetric flooding processes obtained from the model test and the numerical simulation. Compared to the symmetric flooding of two adjacent compartments in Figure 12, the single compartment only allowed the flooding water to flow in a limited space. Therefore, the flooding comparison at the typical moment would be dominated by solid–liquid interactions in the transient flooding stage. Similar to the comparison results in Figure 12, the numerical results in Figure 15 also accurately reproduce the jet flow and interaction behaviors. As for the flashy flow underwater, the overlooking view cannot provide an effective comparative analysis due to the lack of obvious fluctuations in the free surface. In general, combining the results in Figures 12 and 15, regardless of the symmetric or asymmetric flooding scenarios, the reliability of the numerical modeling method in visualizing the flooding process was verified.

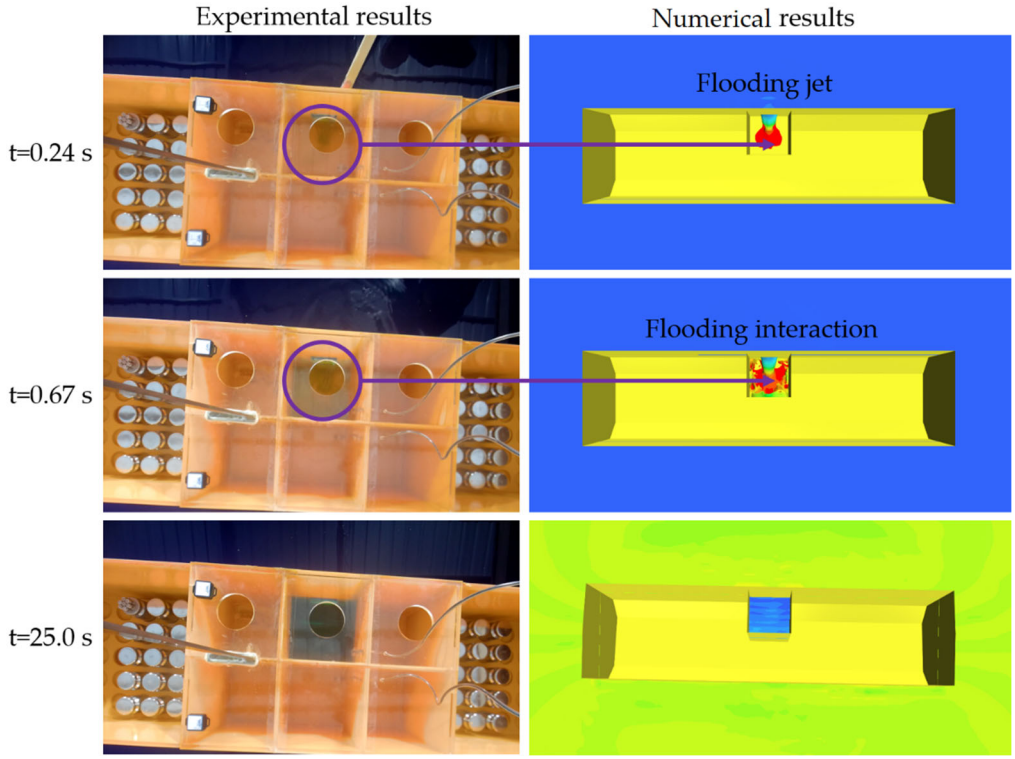

Figure 15. Comparison of asymmetric flooding process between the test and numerical results.

Figure 16 compares the roll motions of the damaged ship in both the model test and numerical simulation. The comparison results show good accuracy in the roll motion curve of the damaged ship, in both the rolling trend and the final heel angle. Asymmetric flooding only accumulated on the damaged side of the ship, gradually worsening the inclining effect with continuous water ingress. The heel angle continued to increase until the flooding ceased, stabilizing the damaged ship at a fixed angle. This also explains the L-shaped curve of the roll motion. Additionally, in terms of the final roll amplitude of the damaged ship, the model test produced a final heel angle of 7.14 degrees, while the numerical simulation provided a value of 7.41 degrees. This small difference of 0.27 degrees resulted in an error of 3.79%. This small comparison error demonstrates the reliability of the numerical modeling method in handling large inclination motions caused by asymmetric flooding.

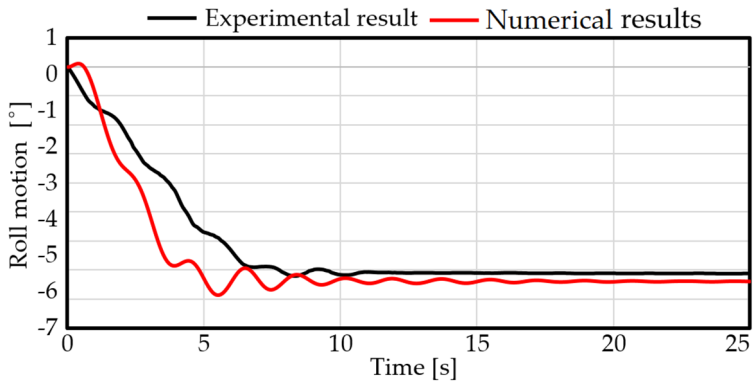

Figure 16. Comparison of roll motions between simulation and test results for asymmetric flooding.

Overall, when comparing the results in Figures 13 and 16, whether in symmetric or asymmetric flooding scenarios, the reliability of the numerical modeling method's reliability in dealing with the motion of the damaged ship is confirmed.

However, when compared with the roll motion of the damaged ship in the symmetric flooding scenario shown in Figure 13, there was a larger discrepancy between the experimental roll curve and the numerical roll curve shown in Figure 16 in the asymmetric flooding scenario. The reasons for this discrepancy can be mainly divided into three aspects. Firstly, continuous asymmetric flooding will gradually increase mesh deformation, resulting in inherent numerical errors. Secondly, the equipment may cause some measurement errors. Thirdly, it can be observed in Figure 16 that during the transient flooding stage, the experimental roll curve mostly lagged behind that obtained by the numerical simulation. In other words, at the same time point, the flooding water in the test compartment was less than in the numerical compartment. This was due to the release mechanism of the damage opening. The approach used in this paper was to glue the tension skin near the damage opening and then release it at the beginning of the test to achieve the transient flooding. However, in actual operation, the tension skin often experiences incomplete release due to uneven tension. This results in a reduced size of the damage opening causing the lagging water ingress in Figure 16. This is also the main factor contributing to the discrepancy between the roll motion curves shown in Figure 16.

There is a need to explain the challenges of using the numerical modelling method when dealing with the motion responses of a damaged ship with different forms of flooding. It is also necessary to clarify the reasons for verifying them individually.

In Section 2.2, it was introduced that whether DFBI rotation and translation or DFBI morphing technique was used for mesh adaption, the free surface may face the problem of moving away from the mesh refinement blocks. This is a common problem. For the DFBI morphing technique applied in this paper, different forms of flooding will lead to different degrees of mesh deformation in the numerical simulation process.

In the case of symmetric flooding discussed in Section 4.1, the mesh deformation in the domain gradually increases during the asymmetric flooding in the early stages. Then, it will gradually reduce due to the subsequent symmetric flooding in the adjacent intact compartment. Finally, under the effects of the symmetric flooding distribution, the mesh in the domain will return to its rectangular configuration in the initial condition.

Regarding the asymmetric flooding in this section, mesh deformation in the domain progressively increases throughout the continuous asymmetric flooding. Until the flooding process is complete, the mesh shape will not further deform. This may pose significant challenges to the numerical modelling method. If the generated heel angle from the asymmetric flooding is too large, the mesh quality with deformation will be poor, resulting in a lower simulation accuracy.

The primary issue is the mesh self-intersection, which can lead to excessively large residual values, hindering the completion of the entire numerical simulation. However, despite these challenges, the simulation validation results in this paper effectively demonstrate the applicability of the DFBI morphing technique.

5. Effect Analysis of Air–Fluid Interaction on Dynamic Responses of the Damaged Ship

In previous studies [10,41], the effects of air compressibility on dynamic responses of damaged ships have been investigated. However, the effects of outflow paths generated by different positions of ventilation holes have rarely been studied, which may affect the accuracy of damage assessment.

To analyze the effects of air–fluid interactions generated by different ventilation positions on the motion of damaged ships, Figures 17–20 numerically compare roll motions in two scenarios: the damage-side ventilation scenario (Case 2) and the intact-side ventilation scenario (Case 3).

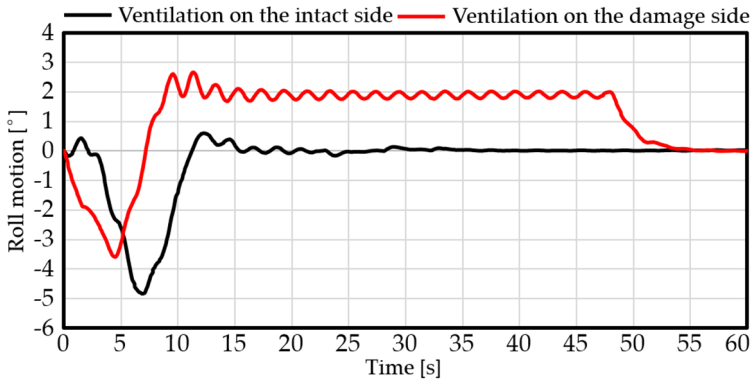

Figure 17. Roll motions of the damaged ship in the 4% ventilation scenario.

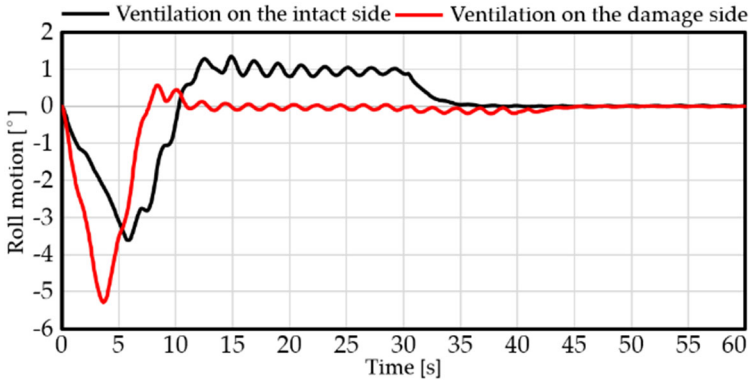

Figure 18. Roll motions of the damaged ship in the 8% ventilation scenario.

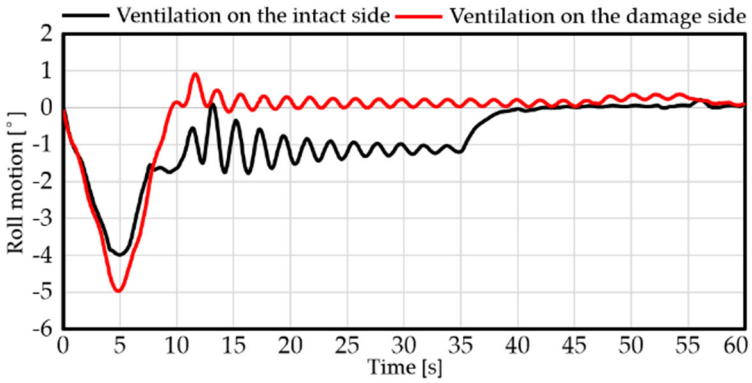

Figure 19. Roll motions of the damaged ship in the 10% ventilation scenario.

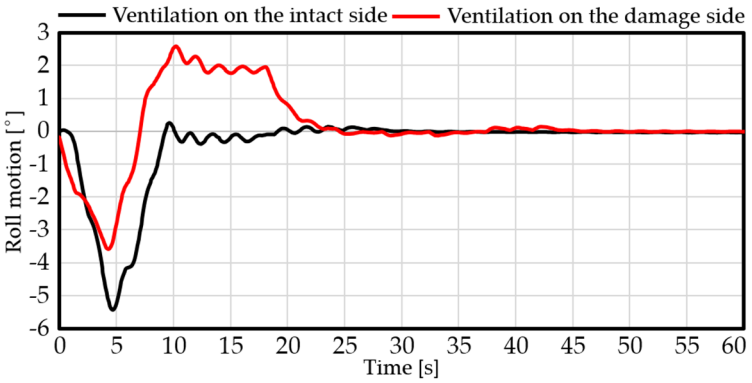

Figure 20. Roll motions of the damaged ship in the 100% ventilation scenario.

Regarding the overall rolling trend, the inherent compartment layout initially causes the damaged ship to incline towards the damaged side, and it gradually return to a positive floating state.

When comparing the rolling details, it is crucial to note that not only is the compressibility of air generated by different ventilation levels significant in damage evaluation, but also the ventilation position. Different ventilation positions alter the interaction mode between compressed air and flooding water, thereby changing the dynamic motion characteristics of the damaged ship.

Overall, the test results in this section underscore the importance of ventilation position in damage evaluation. However, they do not conclusively determine which ventilation mode is more beneficial for the dynamic stability of damaged ships due to the limitations of the test results.

As shown in Figure 21, even with a 10% ventilation level, the change in the velocity field mainly concentrated in the vicinity of the ventilation hole. In this case, the air–fluid interactions in the flooding region became ineffective. Therefore, this section focuses on the 100% ventilation scenarios as the research object and analyze the air–fluid interactions in the flooding compartments, as shown in Figures 22 and 23.

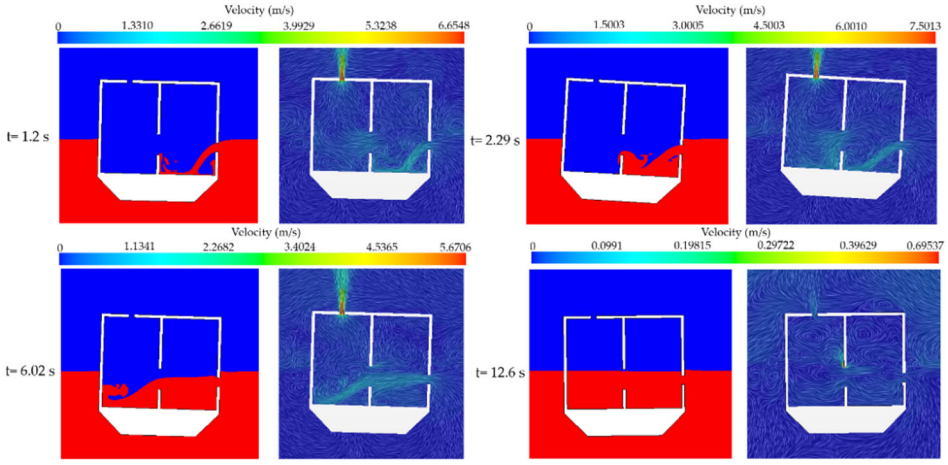

Figure 21. Air–fluid interactions in the intact-side ventilation scenario (10%).

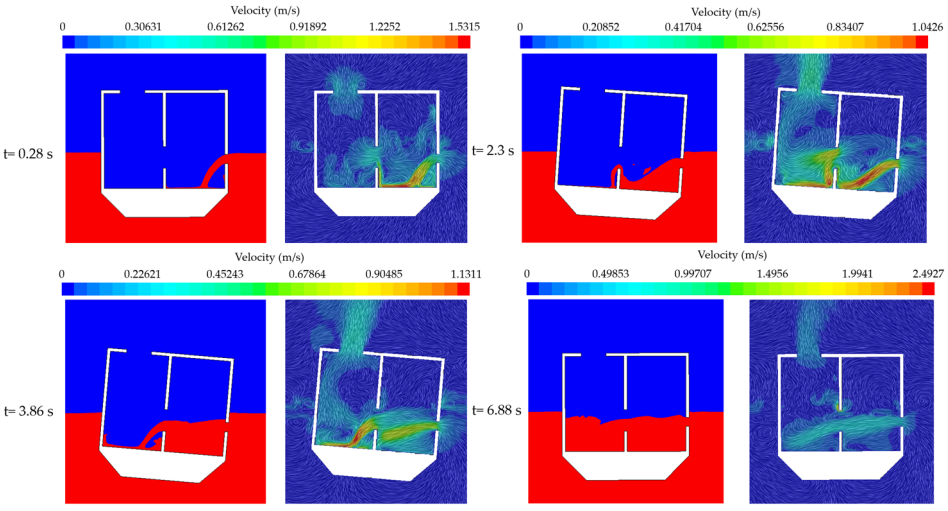

Figure 22. Air–fluid interactions in the intact-side ventilation scenario (100%).

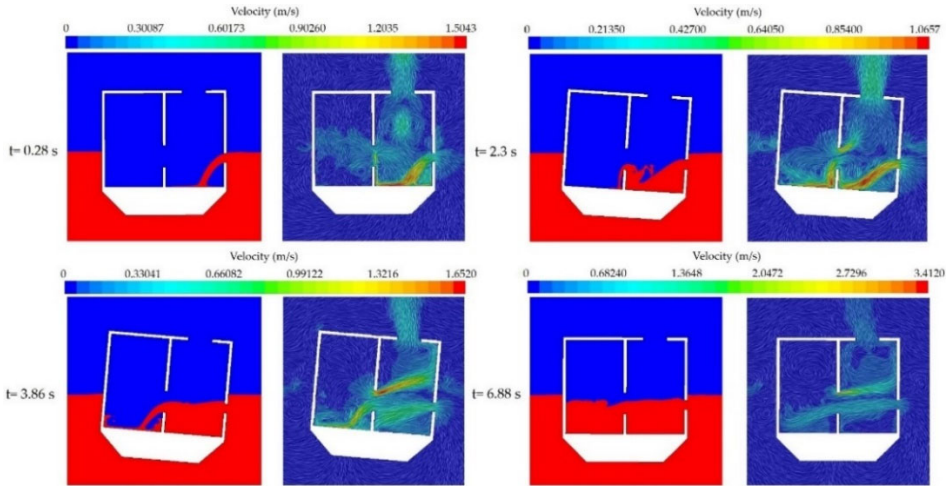

Figure 23. Air–fluid interactions in the damage-side ventilation scenario (100%).

Firstly, it was observed that different ventilation positions generated varying overflow paths for the compressed air. When the ventilation hole was set on the intact side, the compressed air in the damaged compartment flowed from there into the intact compartment along with the flooding water. Subsequently, it overflowed through the ventilation hole along with the air in the intact compartment. The overall overflow process was not restricted by the space. As depicted in Figure 22, there were no violent interactions between the overflowing air and the flooding water.

However, when the ventilation hole is placed on the damaged side, the compressed air in the damaged compartment can directly overflow from the ventilation hole, facilitating the flooding process. This also explains why the maximum roll amplitude in the damaged-side ventilation scenario appeared earlier than that in the intact-side ventilation scenario, as shown in Figures 17–20.

In the intact compartment, the overflow of compressed air will share with the internal opening in the longitudinal bulkhead by the flooding flow. As shown in Figure 23, the close intact compartment and reverse overflow in the internal opening resulted in violent air–fluid interactions.

By comparing the flooding process and the velocity fields in Figures 22 and 23, it becomes evident that at the same flooding moment, different air–fluid interaction behaviors altered the micro-hydrodynamic details of the flooding. Consequently, the moment of inclination generated by the flooding water will produce different motion responses for the damaged ship.

Moreover, due to the different positions of the ventilation holes, the overflow of compressed air generates different forms of acting forces on the internal hull. As shown in Figure 22, the overflowing air constantly acted on the intact side of the damaged ship, whereas in Figure 23, it constantly acted on the damaged side. This explanation also elucidates why the damaged hull in Figures 17–20 exhibited different roll motions. In summary, the visualized numerical results greatly aid in explaining the experimental results. In general, the above explanation based on the velocity field can effectively indicate effects of air–fluid interaction on the motion response of the damaged ship. This introduces a new consideration factor to the damage assessment of the ship.

6. Conclusions and Future Works

This paper focuses on the validation analysis of the numerical method for simulating on the transient flooding of the damaged ship. It provides detailed insights into the numerical approach based on the CFD code STAR-CCM+, with a particular emphasis on the application of user-defined functions (UDFs). These functions are crucial for realizing transient flooding simulations. Additionally, the paper outlines the experimental campaign, including the test scenario and the test model. Notably, the innovation lies in the design of

a function that enables a single operator to record both the flooding process and motion responses of the damaged ship, streamlining the experimental process.

The introduced numerical and experimental techniques offer valuable references for future studies on damaged ships. By comparing the experimental and numerical results, the reliability of the numerical modelling method is confirmed from two perspectives. Firstly, the visualization capability of the volume of fluid (VOF) method is validated through the accurate representation of hydrodynamic phenomena such as jet flow, body-fluid interactions, and mixing flow in multiple compartments. Secondly, the accuracy of the dynamic fluid–body interaction (DFBI) morphing technique in handling mesh adaptation is confirmed through the roll motion of the damaged ship, with the error in roll amplitude controlled within 4%.

Building upon the verified numerical method, the paper proceeded to numerically compare the roll motions of damaged ships with different ventilation positions. It was concluded that the air compressibility under different ventilation levels cannot be neglected in damage assessment. Additionally, the air–fluid interactions generated by different ventilation positions must be considered. Microscopic velocity field analysis in scenarios with full ventilation reveals that different ventilation positions produce varying outflow paths of compressed air, resulting in different acting forces on the hull. This introduces a new consideration for ship damage assessment.

The numerical simulations in this paper were performed on a workstation with 12 processors. Taking the fine mesh case as the symmetric flooding scenario, the total physical simulation time took about 140 h, which can provide a good indication for the capabilities of other researchers to reproduce the similar studies.

In further studies, it is suggested that more influencing factors would be investigated, including compartment permeability, actual compartment layout, and external wave excitation, to better understand the remaining survivability of damaged ships in realistic conditions. Moreover, more damage scenarios, including the bottom flooding, are also worthy of further study. In particular, with the development of polar routes, innovative studies on damage flooding in ice regions using feasible and effective numerical methods are warranted.

Author Contributions: Conceptualization, X.Z. and S.M.; data curation, X.Z., S.M. and F.L.; formal analysis, X.Z., S.M. and F.L.; investigation, X.Z., S.M., F.L. and R.Z.; methodology, X.Z. and S.M.; project administration, R.Z.; resources, R.Z.; software, X.Z. and S.M.; supervision, X.Z., S.M. and R.Z.; validation, X.Z. and S.M.; visualization, X.Z., F.L. and R.Z.; writing—original draft, X.Z., S.M., F.L. and R.Z.; writing—review and editing, X.Z., S.M., F.L. and R.Z. All authors have read and agreed to the published version of the manuscript.

Funding: This work was supported by National Natural Science Foundation of China (grant no. 52271318).

Institutional Review Board Statement: Not applicable.

Informed Consent Statement: Not applicable.

Data Availability Statement: Data will be made available on request.

Conflicts of Interest: The authors declare no conflicts of interest.

References

1. Vassalos, D.; Turan, O. A realistic approach to assessing the damage survivability of passenger ships. *Trans.—Soc. Nav. Archit. Mar. Eng.* **1994**, *102*, 367–394.
2. Lee, D.; Song, S.Y.; Lee, G.J. Theoretical and experimental study on dynamic behavior of a damaged ship in waves. *Ocean Eng.* **2007**, *34*, 21–31. [CrossRef]
3. Santos, T.A.; Guedes Sores, C. Numerical assessment of factors affecting the damaged ro-ro ships in waves. *Ocean Eng.* **2009**, *36*, 797–809. [CrossRef]
4. Spanos, D.; Papanikolaou, A. On the time dependence of survivability of ROPAX ships. *J. Mar. Sci. Technol.* **2012**, *17*, 40–46. [CrossRef]

5. Acanfora, M.; Cirillo, A. A simulation model for ship response in flooding scenario. *Proc. Inst. Mech. Eng. Part M J. Eng. Marit. Environ.* **2017**, *231*, 153–164. [CrossRef]
6. Chang, B.C. On the damage survivability of ro-ro ships investigated by motion simulation in a seaway. *Ship Technol. Res.* **1999**, *46*, 192–207.
7. Manderbacka, T.; Ruponen, P.; Kulovesi, J.; Matusiak, J. Model experiments of the transient responses to flooding of the box shaped barge. *J. Fluids Struct.* **2015**, *57*, 127–143. [CrossRef]
8. Rodrigues, J.M.; Lavrov, A.; Hinostroza, M.A.; Guedes Soares, C. Experimental and numerical investigation of the partial flooding of a barge model. *Ocean Eng.* **2018**, *169*, 586–603. [CrossRef]
9. Siddiqui, M.A.; Greco, M.; Lugni, C.; Faltinsen, O.M. Experimental studies of a damaged ship section in forced heave motion. *Appl. Ocean Res.* **2019**, *88*, 254–274. [CrossRef]
10. Ruponen, P.; Kurvinen, P.; Saisto, I.; Harras, J. Air compression in a flooded tank of a damaged ship. *Ocean Eng.* **2013**, *57*, 64–71. [CrossRef]
11. IMO. *Resolution MSC.245 (83): Recommendation on a Standard Method for Evaluating Cross-Flooding Arrangements*; Adopted 12 October 2007; IMO, 2007.
12. Korkut, E.; Altar, M.; Incecik, A. An experimental study of motion behavior with an intact and damaged Ro-Ro ship model. *Ocean Eng.* **2004**, *31*, 483–512. [CrossRef]
13. Lee, S.; You, J.M.; Lee, H.H.; Lim, T.; Rhee, S.H.; Rhee, K.P. Preliminary tests of a damaged ship for CFD validation. *Int. J. Nav. Arch. Ocean Eng.* **2012**, *4*, 172–181. [CrossRef]
14. Domeh, V.D.K.; Sobey, A.J.; Hudson, D.A. A preliminary experimental investigation into the influence of compartment permeability on damaged ship response in waves. *Appl. Ocean Res.* **2015**, *52*, 27–36. [CrossRef]
15. Santos, T.A.; Winkle, I.E.; Guedes Soares, C. Time domain modelling of the transient asymmetric flooding of Ro-Ro ships. *Ocean Eng.* **2002**, *29*, 667–688. [CrossRef]
16. Lim, T.; Seo, J.; Park, S.T.; Rhee, S.H. Free-running model tests of a damaged ship in head and following seas. In Proceedings of the 12th International Conference on the Stability of Ships and Ocean Vehicles, Glasgow, UK, 14–19 June 2015.
17. Bašić, J.; Degiuli, N.; Dejhalla, R. Total resistance prediction of an intact and damaged tanker with flooded tanks in calm water. *Ocean Eng.* **2017**, *130*, 83–91. [CrossRef]
18. Acanfora, M.; Luca, F.D. An experimental investigation into the influence of the damage opening on ship response. *Appl. Ocean Res.* **2016**, *58*, 62–70. [CrossRef]
19. Lee, Y.; Chan, H.S.; Pu, Y.; Incecik, A.; Dow, R.S. Global Wave Loads on a Damaged Ship. *Ships Offshore Struct.* **2012**, *7*, 237–268. [CrossRef]
20. Begovic, E.; Day, A.H.; Incecik, A. An experimental study of hull girder loads on an intact and damaged naval ship. *Ocean Eng.* **2017**, *133*, 47–65. [CrossRef]
21. Begovic, E.; Mortola, G.; Incecik, A.; Day, A.H. Experimental assessment of intact and damaged ship motions in head, beam and quartering seas. *Ocean Eng.* **2013**, *72*, 209–226. [CrossRef]
22. Ćatipović, I.; Ćorak, M.; Parunov, J.; Alujević, N. Seakeeping experiments on damaged ship. *Ships Offshore Struct.* **2019**, *14*, 100–111. [CrossRef]
23. Jalonen, R.; Ruponen, P.; Weryk, M.; Naar, H.; Vaher, S. A study on leakage and collapse of non-watertight ship doors under floodwater pressure. *Mar. Struct.* **2017**, *51*, 188–201. [CrossRef]
24. Begovic, E.; Day, A.H.; Incecik, A.; Mancini, S.; Pizzirusso, D. Roll damping assessment of intact and damaged ship by CFD and EFD methods. In Proceedings of the 12th International Conference on the Stability of Ships and Ocean Vehicles, Glasgow, UK, 14–19 June 2015.
25. Zhang, X.L.; Lin, Z.; Mancini, S.; Li, P.; Liu, D.K.; Liu, F.; Pang, Z.W. Numerical investigation into the effect of damage openings on ship hydrodynamics by the overset mesh technique. *J. Mar. Sci. Eng.* **2020**, *8*, 11. [CrossRef]
26. Zhang, X.L.; Lin, Z.; Li, P.; Liu, D.K.; Li, Z.; Pang, Z.W.; Wang, M.Q. A numerical investigation on the effect of symmetric and asymmetric flooding on the damage stability of a ship. *J. Mar. Sci. Technol.* **2020**, *25*, 1151–1165. [CrossRef]
27. Gao, Z.L.; Wang, Y.; Su, Y.; Chen, L. Numerical study of damaged ship's compartment sinking with air compression effect. *Ocean Eng.* **2018**, *147*, 68–76. [CrossRef]
28. Sadat-Hosseini, H.; Kim, D.H.; Carrica, P.M.; Rhee, S.H.; Stern, F. URANS simulations for a flooded ship in calm water and regular beam waves. *Ocean Eng.* **2016**, *120*, 318–330. [CrossRef]
29. Haro, M.P.E.; Seo, H.J.; Sadat-Hosseini, H.; Seok, W.C.; Rhee, S.H.; Stern, F. Numerical simulations for the safe return to port of a damaged passenger ship in head or following seas. *Ocean Eng.* **2017**, *14*, 305–318. [CrossRef]
30. Ming, F.R.; Zhang, A.M.; Cheng, H.; Sun, P.N. Numerical simulation of a damaged ship cabin flooding in transversal waves with Smoothed Particle Hydrodynamics method. *Ocean Eng.* **2018**, *165*, 336–352. [CrossRef]
31. Gao, Z.L.; Wang, Y.; Su, Y. On damaged ship motion and capsizing in beam waves due to sudden water ingress using the RANS method. *Ocean Eng.* **2020**, *95*, 102047. [CrossRef]
32. Zhang, X.L.; Mancini, S.; Li, P. Numerical investigation into the Effects of Layer and Accumulated Ice Floes on the Hydrodynamics Performance of the Damaged Ship. In Proceedings of the Thirty-Second International Ocean and Polar Engineering Conference, Shanghai, China, 5–10 June 2022.

33. Zhang, X.L.; Lin, Z.; Mancini, S.; Li, P.; Li, Z.; Liu, F. A Numerical Investigation on the Flooding Process of Multiple Compartments Based on the Volume of Fluid Method. *J. Mar. Sci. Eng.* **2019**, *7*, 211. [CrossRef]
34. ITTC. *Procedures and Guidelines: Practical Guidelines for Ship CFD Applications. 7.5-03-02-03*; International Towing Tank Conference, 2011.
35. Mancini, S.; Begovic, E.; Day, A.H.; Incecik, A. Verification and validation of numerical modelling of DTMB 5415 roll decay. *Ocean Eng.* **2018**, *162*, 209–223. [CrossRef]
36. Handschel, S.; Köllisch, N.; Soproni, J.P.; Abdel-Maksoud, M. A numerical method for estimation of ship roll damping for large amplitudes. In Proceedings of the 29th Symposium on Naval Hydrodynamics, Gothenburg, Sweden, 26–31 August 2012.
37. Ubbink, O. Numerical Prediction of Two Fluid Systems with Sharp Interfaces. Doctoral Dissertation, Department of Mechanical Engineering, Imperial College of Science, Technology & Medicine, London, UK, 1997.
38. Muzaferija, S.; Peric, M. Computational of Free Surface Flows Using Interface Tracking and Interface Capturing Methods. In *Nonlinear Water Wave Interaction*; WIT Press: Southampton, UK, 1999.
39. Wackers, J.; Koren, B.; Raven, H.C.; Van der Ploeg, A.; Starke, A.R.; Deng, G.B.; Queutey, P.; Visonneau, M.; Hino, T.; Ohashi, K. Free-Surface Viscous Flow Solution Methods for Ship Hydrodynamics. *Arch. Computat. Methods Eng.* **2011**, *18*, 1–41. [CrossRef]
40. Ruponen, P. Flooding Model Teat for ITTC Benchmarking Study (ITTC-Box). Available online: http://www.shipstab.org/ (accessed on 29 August 2013).
41. Zhang, X.L.; Mancini, S.; Liu, F. Experimental and numerical investigation on effects of air compressibility on dynamic performance of the damaged ship. *Ocean Eng.* **2023**, *287*, 115837. [CrossRef]

Disclaimer/Publisher's Note: The statements, opinions and data contained in all publications are solely those of the individual author(s) and contributor(s) and not of MDPI and/or the editor(s). MDPI and/or the editor(s) disclaim responsibility for any injury to people or property resulting from any ideas, methods, instructions or products referred to in the content.